MODELLING OF GRID FOLLOWING INVERTER FOR PERFORMANCE EVALUATION OF POSITIVE SEQUENCE MEMORY POLARIZED DISTANCE RELAY

Meenu Jayamohan[1], Sarasij Das[2] Jose de Jesus Chavez[3], Marjan Popov[4]*

[1]*Electrical Engineering, Indian Institute of Science, Bangalore, India*
[2]*Electrical Engineering, Indian Institute of Science, Bangalore, India*
[3]*School of Engineering & Sciences, Tecnologico de Monterrey, Guadalajara, Mexico*
[4]*Faculty of EEMCS, Delft University of Technology, Delft, The Netherlands*
**E-mail: sarasij@iisc.ac.in*

Keywords: Distance relay, Grid following inverter, Mho relay, Positive sequence memory polarization, PV

Abstract

Integration of Inverter-Based Resources (IBRs), like Photovoltaic (PV) and Wind Turbine Generator (WTG), into the power grid necessitates accurate inverter models for assessing their dynamic behaviour and interaction with protection functionalities, such as the Positive Sequence Memory Polarized (PSMP) mho distance relay. This research examines the appropriate Grid Following (GFOL) inverter models for the performance evaluation of PSMP mho relay, considering accuracy and computational efficiency, which is lacking in the existing literature. The research meticulously investigates three different GFOL inverter model structures: detailed, average, and generic models. Each model is thoroughly evaluated for its computational burden and accuracy during events. The GFOL PV generators used in this study are equipped with reactive power priority control and incorporate Low Voltage Ride-Through and High Voltage Ride-Through functionalities. A significant finding of this study is that the generic model can adequately simulate the performance of PSMP mho relays. This offers a valuable solution for computationally efficient system-level studies without compromising relay performance accuracy.

1 Introduction

The global transition toward sustainable energy has spurred a significant rise in inverter-based resources (IBRs), such as photovoltaic (PV) systems, as a pivotal component of modern power grids. The increasing penetration of these resources, driven by ambitious renewable energy targets and advancements in photovoltaic technology, necessitates accurate modeling and protection strategies to ensure system stability and reliability. In this context, dynamic models of PV systems—ranging from detailed electromagnetic transient (EMT) representations to simplified phasor domain (PD) models—have been extensively developed to cater to various operational and analytical needs [1]. However, these models often exhibit divergent accuracy and computational demands, especially under dynamic conditions.

Switching models offer a high-fidelity representation of inverter behavior by incorporating detailed characteristics of semiconductor devices. These models enable in-depth studies of inverter efficiency, harmonic performance, DC bus utilization, and the impact of pulse-width modulation (PWM) schemes. However, their computational intensity can be a limiting factor, especially for large-scale system studies. Reduced-order models are commonly employed to balance accuracy and efficiency, simplifying inverter dynamics by replacing switching poles with controllable voltage sources [2]. While reduced-order models facilitate faster simulations and are effective for broader system-level studies, they may overlook critical inverter dynamics, such as those influenced by network impedance and stability. Depending on the study's focus, a trade-off between detailed switching models and reduced-order approximations becomes necessary [3], [4].

PV systems, operating as Grid-Following (GFOL) IBRs, pose unique challenges for protective relays due to their distinct dynamic behavior, particularly in low short-circuit ratio (SCR) scenarios. Unlike synchronous generators (SGs), PV inverters exhibit limited fault current contribution, rapid control-driven responses, and dependency on phase-locked loop (PLL) dynamics. These characteristics necessitate innovative protection schemes capable of distinguishing faults from other transient events while maintaining sensitivity and selectivity. Positive Sequence Memory Polarized (PSMP) mho relays, with their ability to leverage memory voltage and current profiles, have been widely used for detecting close-in faults in transmission lines. However, there is limited existing literature that analyzes the adequacy of full, average, and generic models of GFOL PV during performance evaluation of PSMP mho relays [5], [6], [7].

https://doi.org/10.1049/icp.2025.1044

While detailed EMT simulations provide unparalleled fidelity in capturing the dynamics of PV systems, their computational intensity limits their applicability to smaller networks. On the other hand, PD simulations, although computationally efficient, often fail to capture high-frequency oscillatory modes and subtle dynamic interactions inherent to IBRs [2]. This trade-off between model accuracy and computational feasibility becomes particularly critical during fault scenarios, where precise representation of inverter dynamics, including inner current control loops and PLL behavior, is essential. Furthermore, discrepancies between EMT and PD models have been reported in weak grid conditions, where algebraically derived voltage transients can misrepresent inverter responses [1].

A critical gap present in the existing literature regarding the impact of various GFOL inverter models on the performance of PSMP mho relays, which are essential for fault detection and protection in power systems. This study aims to address this knowledge gap by investigating the influence of different inverter models on PSMP mho relay behaviour under various fault scenarios and Short Circuit Ratio (SCR) conditions. This study utilizes simulations on an IEEE 39 bus system to analyze the response of PSMP mho relays to a three GFOL inverter models and fault scenarios. Simulations encompass various fault scenarios, including single-line-to-ground (SLG), line-to-line (LL), and three-phase-to-ground faults (LLLG) occurring at diverse locations within the system, along with varying fault resistances. The influence of Phase-Locked Loop (PLL) types and control parameters employed in GFOL inverters are investigated, as PLL dynamics can impact relay behaviour during fault events. SCR ratios are varied to examine their effect on PSMP mho relay operation for all three models of GFOL PV. By analyzing the dynamic response and fault detection capabilities of these relays across different modeling paradigms, this study seeks to establish a comprehensive understanding of their applicability and limitations. The outcomes of this work provide valuable insights on the adequacy of GFOL PV models during performance evaluation of PSMP mho relays. The contributions of the paper are listed below.

- By comparing the relay's behavior across the different GFOL inverter model structures, the adequacy and limitations of each model are assessed.
- The performance evaluation of PSMP mho relays within these different model structures reveals nuanced impacts on relay operation and coordination.
- This study examines the effects of different inverter models on PSMP mho relay behavior under various fault scenarios.
- The impact of PLL dynamics on the PSMP mho relay is also analyzed using the different inverter models.
- Notably, our findings indicate that the generic model can adequately simulate the performance of memory-polarized mho relays in most scenarios, offering a practical solution for system-level studies without compromising critical relay performance characteristics.

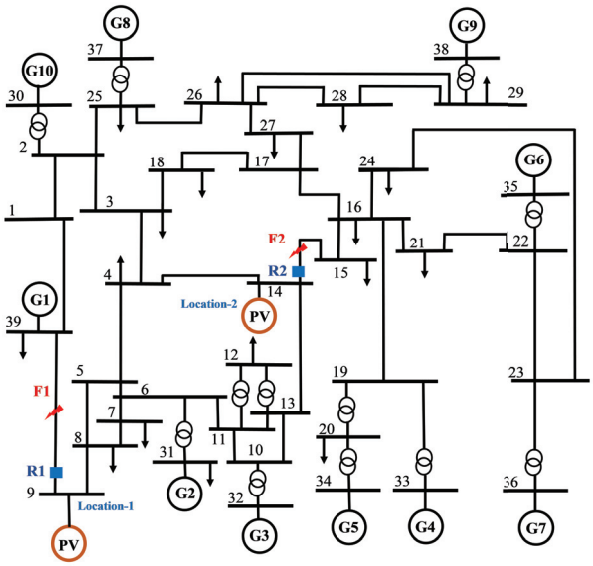

Fig. 1. Modified IEEE 39 bus system

2 Investigated Models

A modified IEEE-39 bus system, with a 47.12 MVA PV plant integrated, is depicted in Fig. 1. To maintain grid stability, the terminal voltage at the Reference Point of Applicability (RPA) must remain within an acceptable range, typically between 0.9 and 1.05 p.u. under normal operating conditions. In this steady-state scenario, the reference active and reactive power values, P_{ref} and Q_{ref}, respectively, are set equal to their respective setpoints, P_{set} and Q_{set}. The P_{set} value can be determined by either the Maximum Power Point Tracker (MPPT) or the Power Plant Controller (PPC). A Synchronous Reference Frame PLL with a Low Pass Filter (LSRF PLL) is used for the studies. The PV inverter operates in reactive power (Q) priority mode, incorporating Low Voltage Ride-Through (LVRT) and High Voltage Ride-Through (HVRT) functionalities along with dynamic voltage support capabilities. During disturbances, the voltage support function is activated, enabling the inverter to provide reactive power support as per grid code requirements. This is provided using the K-factor, which is considered as two throughout the work. The inverter's maximum output current is limited to 1.2 p.u. [8], [7]. The PQ control implementation in this study is based on dq positive sequence. The three different PV models considered are designed to have the same MVA ratings and functionalities as described. The different models are connected to the IEEE 39 bus system via a transmission line of impedance Z_{pv}, which is $0.0043 + 0.0474j$ p.u./m.

2.1 Ful Converter or Detailed Model

This aggregated PV model, often termed an EMT model, is suitable for simulations spanning microseconds to seconds [9]. EMT simulations typically necessitate mathematical models expressed algebraically or through differential equations solved via implicit integration methods. To mitigate the computational

burden in large-scale PV plants, reduced-order models employing scaled-down representations of individual PV units are commonly employed. These models significantly decrease the model size and calculation time, proving invaluable for design, simulation, and control strategy verification [2]. This full converter / detailed model captures full inverter dynamics for high-fidelity representation. It accurately captures high-frequency switching transients and interactions between the GFOL system and the grid but at the cost of significant computational resources and time [10].

A detailed model representation of the grid-connected PV is shown in Fig. 2. The control architecture for this detailed model is depicted in Fig. 3. The outer PQ control loops compare the desired real and reactive power references with the actual power outputs, generating corresponding d-axis and q-axis current references (i_{dref} and i_{qref}). As shown in Fig. 3, these current references are subject to constraints imposed by limiters L_1, L_3, derived according to the methodology outlined in [2] and [11]. Limiters L_2 and L_4 constrain the modulation signals. The inner current control loops compare the reference currents with the actual d-axis and q-axis measured currents. Feed-forward compensation is employed to decouple the inner current loops using the d-axis and q-axis components of V_{rpa} (v_d and v_q). The DC-link voltage (V_{dc}) compensates for the converter voltage gain and subsequently generates the modulation signals, d_d, and d_q. Finally, these modulation signals are processed by the Pulse Width Modulation (PWM) block to generate the switching signals for the inverter [12].

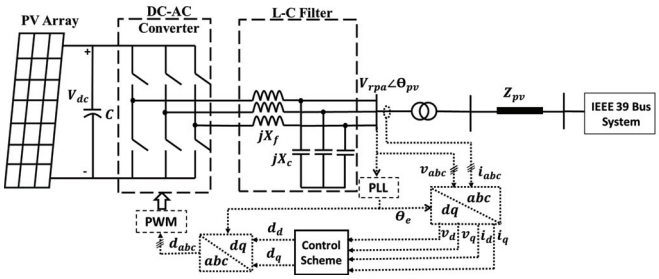

Fig. 2. Full converter model of grid-connected PV system

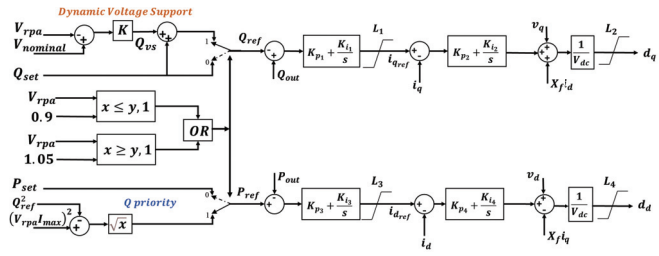

Fig. 3. Control scheme for full and average model PV system

2.2 Average Model

In EMT studies of power systems with multiple PV plants, detailed PV models can significantly increase simulation times, often requiring tens of minutes to simulate several seconds of system dynamics [13]. When accurate representation of harmonics near switching frequencies is not the primary objective, the high-frequency switching behaviour of power electronic converters can be simplified through techniques such as circuit averaging, state-space averaging, or their advanced variants [3], [14], [15].

In a typical representation of such an averaged model, as shown in Fig. 4, the inverter within the aggregated PV unit is modelled as an equivalent voltage source, producing the AC voltage averaged over a single switching cycle [2], [9]. While average model omits the detailed Fault Ride Through control strategies, it effectively captures the dynamic interactions between controllers and the broader power system [16]. This averaging approach enables the use of significantly larger time steps (typically $50\mu s$), enabling the efficient simulation of several seconds of system dynamics [15]. Hence, the average model achieves a balance between accuracy and efficiency by averaging inverter dynamics over a switching cycle. Here, the control architecture used is the same as that used for the detailed model. However, the v_{dref} and v_{qref} obtained from the control loops are transformed to obtain reference voltages for the three phases and are subsequently applied to the control voltage sources [2], [12].

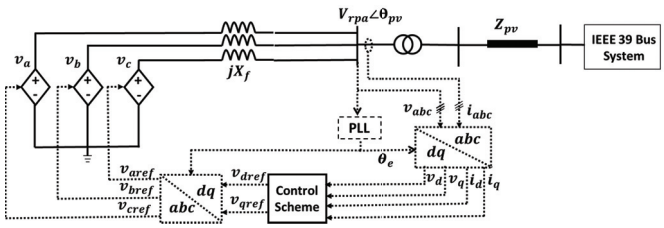

Fig. 4. Average model of grid-connected PV system

2.3 Generic Model

For system-level analyses, where dominant dynamics of PV plants are of primary concern, simplified models are often employed. These models abstract away the detailed internal topology of the PV units. The entire PV system can be represented as a controlled current source, effectively filtering out high-frequency dynamics [13]. Notable examples of the simplified representation include GE's phasor model [17], which utilizes only current magnitude and angle at the fundamental frequency, and the generic models developed by WECC in collaboration with EPRI [18], [19]. The WECC PV plant model serves as a representative example of this generic model, as shown in Fig. 5. The details of the generic model are in [18]. This generic model employs phasor quantities, representing sinusoidal voltages and currents at the system's nominal

frequency. As such, it is well-suited for analyzing positive sequence dynamics at the system level [20],[21].

The generic model control architecture is shown in Fig. 6. The generic model represents the GFOL system as a controlled current source, as shown in Fig. 7, enabling efficient simulations for system-level studies. Moreover, its utilization of phasor quantities at the system nominal frequency facilitates positive sequence dynamic analysis. The d-axis and q-axis current command signals are denoted as I_{Pcmd} and I_{Qcmd}, respectively. To mitigate high-frequency noise, the current command signals are filtered through low-pass filters with a time constant (T_g) of 0.02 s, resulting in the filtered d-axis and q-axis current references, I_{pref} and I_{qref}, respectively. The control system utilizes Proportional-Integral (PI) controllers with the following parameters: for the outer reactive power (Q) loop, K_{p5}=0.05 and K_{i5}=1; for the inner reactive power loop, K_{p6}=1 and K_{i6}=4. The detailed mathematical formulation of the PV model, including its dynamic behavior, control algorithms, and operational characteristics, has been documented in [7], [12].

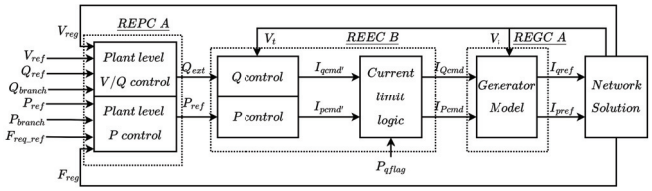

Fig. 5. WECC generic model block diagram

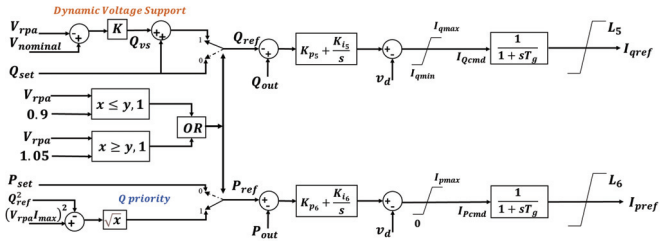

Fig. 6. Control scheme for generic model PV system

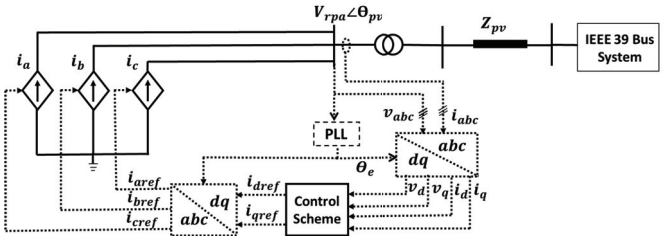

Fig. 7. Generic model of grid-connected PV system

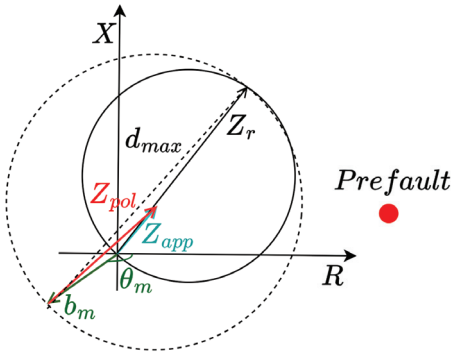

Fig. 8. Dynamic mho expansion for SG-only system

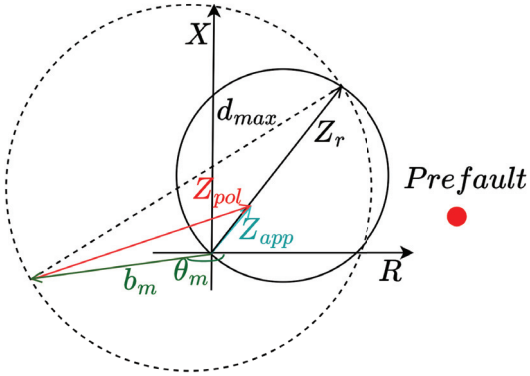

Fig. 9 Dynamic mho expansion for GFOL PV integrated system

3 PSMP Mho Relay

PSMP mho relays enhance the reliability of mho relays during close-in faults by employing pre-fault positive-sequence voltage for polarization, overcoming the limitations of self-polarized mho relays. This memory-based approach dynamically expands the mho characteristic, significantly impacting relay performance. Over time, the memory voltage gradually converges towards the actual fault voltage. The dynamic expansion is characterized by the memory vector (b_m), calculated as the difference between the apparent impedance (Z_{app}) and the polarizing impedance (Z_{pol}). The diameter of the dynamic mho expansion is d_m.

$$b_m(i) = Z_{app}(i) - Z_{pol}(i); \;\; d_m(i) = |Z_r(i) - b_m(i)| \quad (1)$$

$$Z_{app}(i) = \frac{V_f(i)}{I_f(i)}; \qquad Z_{pol}(i) = \frac{V^+_{f,m}(i)}{I_f(i)} \quad (2)$$

where I_f is the fault current and $V^+_{f,m}$ is the positive sequence memory voltage or pre-fault voltage. The memory voltage, updated iteratively, is defined as:

$$V^+_{f,m}(i) = \omega_m . V^+_f(i) + (1 - \omega_m) . V^+_{f,m}(i - j) \quad (3)$$

where V^+_f denotes the positive sequence faulted phase voltage phasor and ω_m is the weight factor. The maximum extent of this

dynamic expansion, denoted as d_{max}, significantly enhances the relay's resistive reach and its ability to correctly identify fault conditions. The angle of the memory vector corresponding to the maximum dynamic mho expansion is denoted as θ_m. The detailed explanation of the Positive Sequence Memory Polarized (PSMP) mho relay and its operational behavior, including its dynamic expansion and memory polarization mechanism, has been extensively studied in [22], [5], [7].

3.1 Comparison of Dynamic Mho Expansion for SG-only system and PV-integrated system

During close-in faults, SGs behave as voltage sources. Due to inertia, the voltage phase angle remains largely unchanged. In an SG-only system, Z_{pol} exhibits low magnitude due to low pre-fault voltage and high fault current, resulting in Z_{app} with small magnitude near the positive R-axis (Fig. 8). This leads to a small b_m value, closely aligning the dynamic mho expansion with the actual mho circle.

In a GFOL PV-integrated system, power electronics limit the fault current and converter control causes fault voltage with reduced magnitude and shifted phase angle. While Z_{app} remains low and near the positive R-axis, Z_{pol} exhibits magnitude and angle closer to pre-fault impedance. Consequently, b_m is significantly longer with a larger angle (θ_m) compared to the SG-only system (Fig. 9), reducing its resistive reach [23], [24], [7]. However, the initial dynamic mho expansion is substantially larger than that in the SG-only system.

In this work, a higher θ_m value indicates that the memory vector (b_m) moves further away from the positive R-axis or negative X-axis and vice versa. Memory vector angle θ_m is measured counterclockwise from the positive R-axis, as illustrated in Figures 8 and 9.

Table 1 presents the polarizing quantities for positive-sequence memory polarization for the considered fault types. Subscripts 'A', 'B', and 'C' denote phases A, B, and C, respectively, where zero sequence compensation factor K_0=0.5 and a=1$\angle$120° [22]. The superscript '+' signifies the positive-sequence component, while the subscript 'm' denotes the memory component.

Table 1 Polarizing quantities of relay elements

Fault Type	Relay element	Fault voltage (V_f)	Positive sequence memory pol:	
			Polarizing voltage	Fault current (I_f)
Three-phase-to-ground	AG	V_A	$V^+_{f,m}$	I_A
Single-line-to-ground	AG	V_A	$V^+_{f,m}$	$I_A + K_0 \cdot I_0$
Line-to-line	AB	$V_A - V_B$	$-j \cdot a \cdot V^+_{f,m} \cdot \sqrt{3}$	$I_A - I_B$

4 Results

Results are generated for three different GFOL PV models- full converter, average, and generic models- for close-in faults (LLLG, SLG, and LL) of duration 0.07 s at a distance of 2%from the bus where the PV is connected to IEEE 39 bus system. For Location-1, PV is connected to Bus 9 with the fault on line 9-39 with the relay $R1$ seeing the fault. For Location-2, the PV is connected to Bus 14 with fault on line 14-15 with corresponding relay $R2$. Fault simulations were executed at a sampling frequency of 3.84 kHz, capturing 64 data points per cycle. Extracted fault data underwent subsequent computational processing. The analysis encompassed eight distinct protection passes within each cycle. To establish the memory voltage for the preceding two cycles, the parameter 'j' was assigned a value of 16 within the memory voltage calculation equations, as defined in (3). This research investigates the maximum achievable expansion of the dynamic mho characteristic of the PSMP mho element and its corresponding memory vector angle within a PV-integrated system. The objective is to comprehensively understand the reduction in resistive reach during various fault scenarios across three distinct PV system models. All the results are for PV connected at Location-1 with LSRF PLL (K_p=50, K_i=200 corresponding to a bandwidth of 8.4 Hz) unless otherwise specified.

4.1 Different fault scenarios

This analysis investigates the maximum dynamic mho expansion (d_{max}) and corresponding memory vector angle (θ_m) for various fault scenarios with zero fault resistance (R_f) utilizing an LSRF PLL with a weight factor (ω_m) of 0.5. Three fault types were considered: LLLG, SLG, and LL. Previous research has demonstrated that the PSMP mho relay's dynamic expansion diminishes in the presence of IBRs [24], [7]. The findings, presented in Figs. 10(a), 10(b), and 10(c), corroborate this observation. The reduction in resistive reach compared to the self-polarized mho circle is zoomed in and shown in all the result figures. Crucially, all three models – full, average, and generic – consistently exhibit comparable maximum expansion and resistive reach reduction across all fault scenarios. The d_{max} for the full model is observed to be the highest, followed by the average model and generic model. The θ_m measured from the positive R-axis is highest for the generic model, which results in its shift to the left more than the other two models, resulting in a slightly more resistive reach reduction. For the LLLG fault, the full model exhibits the highest resistive reach, with the average model demonstrating a 0.1 Ω reduction and the generic model exhibiting a further reduction of 1 Ω on the positive R-axis. For the SLG fault, the resistive reach difference is around 1.5 Ω, and for the LL fault, it is around 1 Ω for generic model with respect to full and average models. While these minor discrepancies exist, they have been observed to be insignificant in terms of relay maloperation during close-in fault studies. These results, validated across all three fault types, unequivocally demonstrate that the generic model effectively replicates the behavior of the full model. Therefore, the generic model can be employed as a suitable surrogate for the full model, significantly reducing the computational burden without compromising the accuracy of the analysis.

4.2 Different fault resistances

To further validate the efficacy of the generic model, simulations were conducted for fault resistances of 5 Ω. The d_{max} for

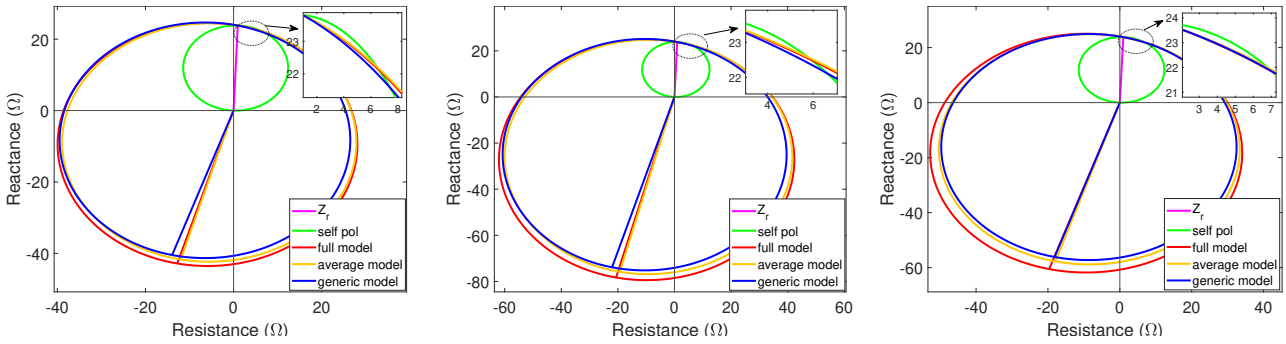

(a) (b) (c)

Fig. 10. Maximum dynamic mho expansion for seen by relay $R1$ for R_f=0 Ω during (a) LLLG fault (b)SLG fault (c)LL fault

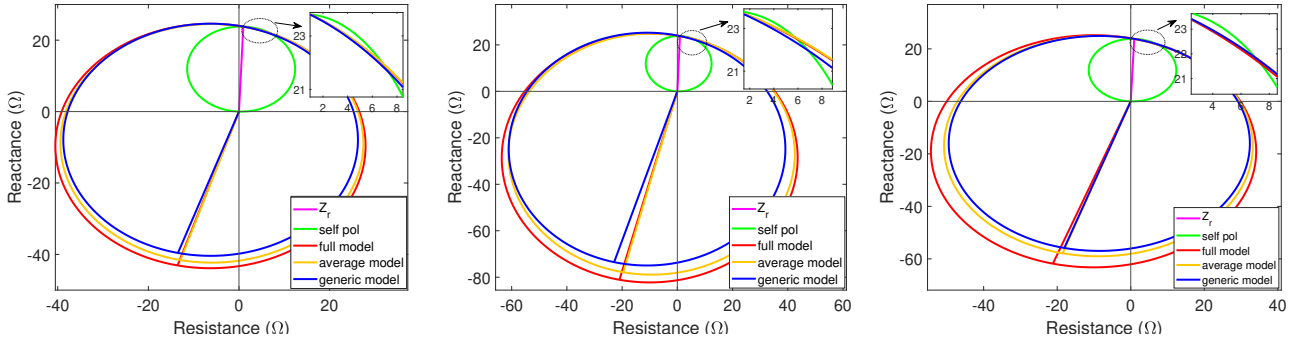

(a) (b) (c)

Fig. 11. Maximum dynamic mho expansion for seen by relay $R1$ for R_f=5 Ω during (a) LLLG (b) SLG (c)LL faults

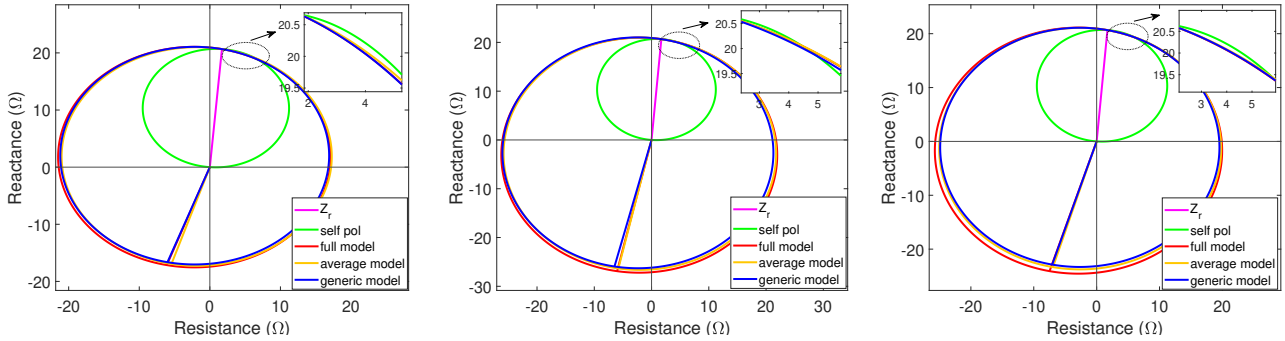

(a) (b) (c)

Fig. 12. Maximum dynamic mho expansion for seen by relay $R2$ for R_f=0 Ω during (a) LLLG (b) SLG (c)LL faults

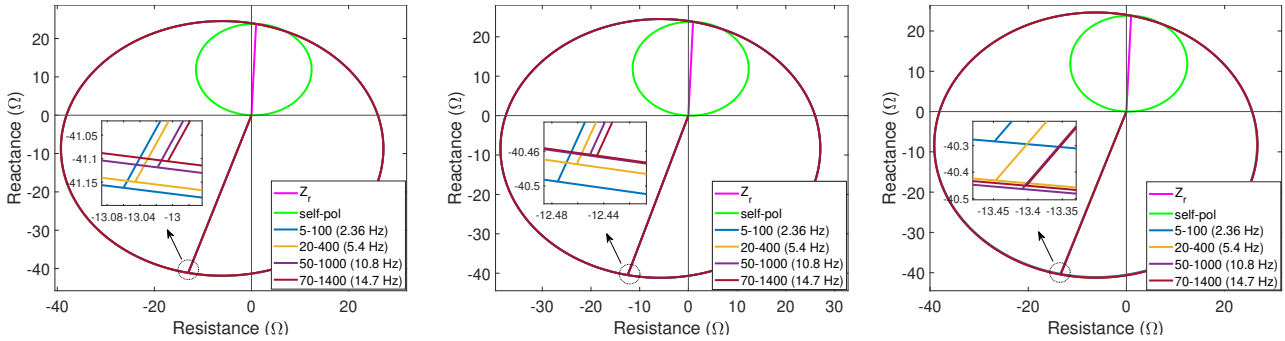

(a) (b) (c)

Fig. 13 Maximum dynamic mho expansion for varying PLL bandwidth seen by relay $R1$ during LLLG fault with R_f=0 Ω for (a) full model (b) average model (c) generic model

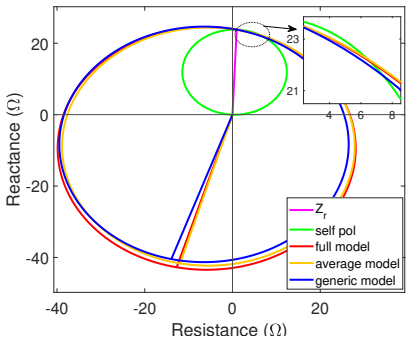

Fig. 14 Maximum dynamic mho expansion for seen by relay $R1$ for R_f=0 Ω during LLLG fault for DSOGI PLL

each fault case is presented in Figs. 11(a), 11(b), and 11(c). It is observed that while the resistive reach of the full and average models are relatively similar, the generic model exhibits a significantly reduced reach, with the difference approaching a value close to 1 Ω. Across all three fault types (LLLG, SLG, and LL), the full, average, and generic models consistently exhibited performance comparable to the previous case with zero R_f. While minor variations were observed, they did not have a discernible impact on relay performance. These findings reinforce the conclusion that the generic model accurately replicates the behavior of the full model, even in the presence of varying fault resistances, making it a reliable and computationally efficient alternative for a wide range of fault scenarios.

4.3 Different locations

To comprehensively assess the model's accuracy, simulations were conducted at different locations within the IEEE 39 bus system- Location-1 and Location-2, as shown in Fig. 1. Consistent with previous observations, the full model exhibits the highest resistive reach. The average model demonstrates a maximum 0.1 Ω reduction, and the generic model shows a further 0.5 Ω decrease in resistive reach along the positive R-axis. The reduction Across a spectrum of fault types (LLLG, SLG, and LL) and fault resistances (0 and 5 Ω), the generic model consistently demonstrated remarkable consistency with the full model. Despite exhibiting slight deviations, their impact on relay performance was negligible, underscoring the model's robustness and its suitability for accurate and efficient fault studies across diverse scenarios within complex power systems. The results for LLLG, SLG, and LL faults with zero R_f at Location-2 seen by relay $R2$ are presented in Fig. 12(a), Fig. 12(b), and Fig. 12(c), respectively.

4.4 Different PLL types and parameters

To further bolster the robustness of these findings, the analysis was extended to encompass different PLL implementations. The maximum dynamic mho expansion for an LLLG close-in fault was verified for both LSRF and Dual Second-Order Generalized Integrator (DSOGI) PLL types for a bandwidth of 8.4 Hz [7]. Along the positive R-axis, the full model demonstrates the highest resistive reach, while the average model shows a 0.1 Ω reduction, and the generic model exhibits a further 1 Ω decrease. Consistent with previous observations, all three models exhibited highly comparable results, demonstrating negligible discrepancies in relay performance (see Fig. 14). Furthermore, the analysis was conducted across a range of PLL bandwidths, spanning from 2.36 Hz to 14.7 Hz for a DSOGI PLL. The difference in resistive reach in the positive R-axis for varying bandwidth has been observed to be in the range of 0.0002 Ω, 0.0005 Ω, and 0.01 Ω for full, average, and generic models, respectively. For each corresponding bandwidth across the models, the full model has the highest resistive reach followed by the average model and generic model as observed in results in Section 4.1. Though the difference in resistive reach is negligible, it has been observed that θ_m decreases as bandwidth increases for the three models studied, as shown in Fig. 13(a), Fig. 13(b), and Fig. 13(c). A detailed study on the variation of PLL parameters on the dynamic mho expansion in PSMP mho relays is presented in [7] with the generic model. Hence, the generic model consistently maintained accuracy, exhibiting minimal deviations from the more full converter and average models across this bandwidth range. These findings unequivocally demonstrate the versatility and robustness of the generic model, highlighting its suitability for a wide range of PLL configurations and operating conditions.

5 Conclusion

This paper studies the operation of PSMP mho relays by analyzing the diameter of maximum mho expansion and its corresponding memory vector angle. In conclusion, the rigorous investigation of three distinct Grid Following inverter models – detailed, average, and generic – has unequivocally demonstrated that the generic model provides sufficient accuracy and computationally efficient representation of GFOL PV for assessing the performance of PSMP mho relays. Through comprehensive simulations encompassing diverse fault scenarios (LLLG, SLG, LL), fault resistances, different locations within the IEEE 39 bus system, and variations in PLL type and control parameters, the generic model consistently exhibited negligible deviations from the more detailed models. So, generic model of GFOL PV is sufficient for studying the behaviour of PSMP mho relays. This finding has significant implications for power system studies with PSMP mho relays, enabling more computationally efficient analysis while maintaining the necessary level of accuracy.

6 Acknowledgement

This work has been funded by the IISc-TU Delft Joint Seed Fund 2022.

7 References

[1] R. W. Kenyon, B. Wang, A. Hoke, J. Tan, and B. M. Hodge, "Comparison of Electromagnetic Transient and Phasor Dynamic Simulations: Implications for Inverter

Dominated Systems," 2023 IEEE Power and Energy Society Innovative Smart Grid Technologies Conference (ISGT), Washington, DC, USA, 2023, pp. 1-5.

[2] P. Chao, W. Li., X. Liang, Y. Shuai, F. Sun., and Y. Ge, "A comprehensive review on dynamic equivalent modeling of large photovoltaic power plants, " *Solar Energy*, 210, pp.87-100, 2020.

[3] D. Ramasubramanian, W. Wang, P. Pourbeik, E. Farantatos, A. Gaikwad, S. Soni, and V. Chadliev, "Positive sequence voltage source converter mathematical model for use in low short circuit systems," *IET Gener. Transm. Distrib.*, 14: 87-97, 2020.

[4] A. Honrubia-Escribano, E. Gómez-Lázaro, J. Fortmann, P. Sørensen and S. Martin-Martinez, "Generic dynamic wind turbine models for power system stability analysis: A comprehensive review," *Renewable and Sustainable Energy Reviews*, 81, pp.1939-1952, 2018.

[5] A. Radhakrishnan, A. Ghosh, I. R. Sai Priyamvada and S. Das, "Performance of Memory-Polarized Distance Relay in Presence of PV Generator with VdC-Q Control," IEEE Energy Conversion Congress and Exposition (ECCE), Detroit, MI, USA, 2022, pp. 1-8.

[6] P. Pourbeik et al., "A Generic Model for Inertia-Based Fast Frequency Response of Wind Turbines and Other Positive-Sequence Dynamic Models for Renewable Energy Systems," *IEEE Trans. on Energy Convers.*, vol. 39, no. 1, pp. 425-434, March 2024.

[7] M. Jayamohan, S. Das and M. Popov, "Sensitivity of Dynamic Mho Characteristic to PLL Parameters of Grid Following PV," 2024 IEEE International Communications Energy Conference (INTELEC), Bengaluru, India, 2024, pp. 1-6

[8] "IEEE Standard for Interconnection and Interoperability of Inverter-Based Resources (IBRs) Interconnecting with Associated Transmission Electric Power Systems," in IEEE Std 2800-2022, vol., no., pp.1-180, 22 April 2022.

[9] R. Yonezawa et al., "Development of detailed and averaged models of large-scale PV power generation systems for electromagnetic transient simulations under grid faults," 2016 IEEE Innovative Smart Grid Technologies - Asia (ISGT-Asia), Melbourne, VIC, Australia, 2016, pp. 98-104.

[10] I. Abuishmais, Q. Salem, R. Aljarrah, and A. Al-Quraan," A Comparative Study between Reduced-Order and Switching Models of Grid-Following Inverter Interfacing Renewable Energy Sources," *Int. J. Energy Res.*, 8849576, 13 pages, 2023.

[11] C. A. Plet, M. Graovac, T. C. Green and R. Iravani, "Fault response of grid-connected inverter dominated networks," IEEE PES General Meeting, 2010, pp. 1-8.

[12] M. Jayamohan, S. Das, and S. Brahma, "Impedance Trajectories during Stable and Unstable Power Swings in Presence of PQ Control based PV Generations," 2023 IEEE PES General Meeting (PESGM), Orlando, FL, USA, 2023, pp. 1-5.

[13] X. Mao and R. Ayyanar, "Average and Phasor Models of Single Phase PV Generators for Analysis and Simulation of Large Power Distribution Systems," 2009 Twenty-Fourth Annual IEEE Applied Power Electronics Conference and Exposition, Washington, DC, USA, 2009, pp. 1964-1970.

[14] A. Davoudi, J. Jatskevich and T. D. Rybel, "Numerical state-space average-value modeling of PWM DC-DC converters operating in DCM and CCM," *IEEE Trans. Power Electron.*," vol. 21, no. 4, pp. 1003-1012, July 2006.

[15] L. Wang et al., "Electromagnetic Transient Modeling and Simulation of Power Converters Based on a Piecewise Generalized State Space Averaging Method," *IEEE Access*, vol. 7, pp. 12241-12251, 2019.

[16] Y. Xu, Y. Chen, C. -C. Liu and H. Gao, "Piecewise Average-Value Model of PWM Converters With Applications to Large-Signal Transient Simulations," *IEEE Trans. Power Electron.*, vol. 31, no. 2, pp. 1304-1321, Feb. 2016.

[17] K. Clark, R. A. Walling, and N. W. Miller, "Solar photovoltaic (PV) plant models in PSLF," 2011 IEEE PES General Meeting, 2011, pp. 1-5.

[18] "WECC solar plant dynamic modeling guidelines," WECC Renewable Energy Modeling Task Force, 2014.

[19] "WECC solar PV dynamic model specification," WECC Renewable Energy Modeling Task Force, 2012.

[20] N. W. Miller, B. Leonardi, R. D'Aquila, et al., "Western Wind and Solar Integration Study Phase 3A: Low Levels of Synchronous Generation," National Renewable Energy Lab.(NREL), 2015.

[21] N. W. Miller, M. Shao, S. Pajic. and R. D'Aquila, "Western wind and solar integration study phase 3–frequency response and transient stability," (No. NREL/SR-5D00-62906). National Renewable Energy Lab(NREL), Golden, CO (United States); GE Energy Management, Schenectady, NY (United States), 2014.

[22] D. D. Fentie, "Understanding the Dynamic Mho Distance Characteristic," in 2016 69th Annual Conference for Protective Relay Engineers (CPRE), IEEE, 2016, pp. 1–15.

[23] B. Kasztenny, "Distance Elements for Line Protection Applications Near Unconventional Sources.", SEL Inc., Nov. 2022

[24] A. Radhakrishnan, I. R. S. Priyamvada and S. Das, "Impact of P – Q Control based PV Generator on Memory-Polarized Mho Relay," 2022 International Conference on Smart Energy Systems and Technologies (SEST), Eindhoven, Netherlands, 2022, pp. 1-6.